Available online at www.sciencedirect.com

ScienceDirect

Mendeleev Commun., 2024, **34**, 640–642

Mendeleev Communications

Precursor method for the synthesis of highly dispersed ZrO_2 doped with scandium

Olga I. Gyrdasova, Rina F. Samigullina, Elena V. Vladimirova, Irina S. Medyankina, Larisa Yu. Buldakova, Mikhail Yu. Yanchenko and Liliya A. Pasechnik*

Institute of Solid State Chemistry, Ural Branch of the Russian Academy of Sciences, 620990 Ekaterinburg, Russian Federation. E-mail: pasechnik@ihim.uran.ru

DOI: 10.1016/j.mencom.2024.09.005

The solid solutions of $Zr_{1-x}Sc_xO_{2-\delta}$ ($0 < x \leqslant 0.1$) were prepared using a precursor technology, and their structural, optical, and photocatalytic characteristics were studied. Mixed formates synthesized by an original method were used as precursors. Scandium favored the formation of ZrO_2 in tetragonal syngony and increased its photoactivity in the UV range.

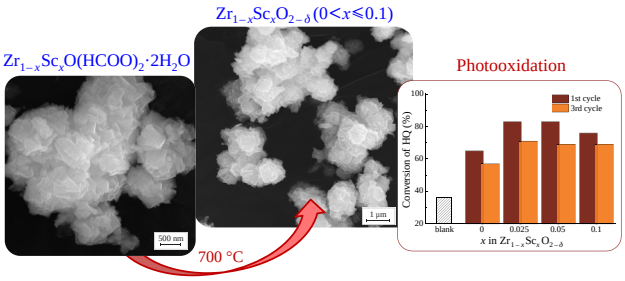

Keywords: zirconium oxide, scandium doping, precursor synthesis, optical spectroscopy, voltammetry, photocatalysis.

Ceramic materials based on Sc-stabilized ZrO_2 have a wide range of promising applications in engineering and medicine due to thermal and chemical resistance, gas tightness, high hardness, *etc*.[1,2] Introduction of foreign metals stabilizes polymorphic ZrO_2 phases (a monoclinic phase is thermodynamically stable from room temperature to 1170 °C; and tetragonal and cubic phases, above 1170 and 2370 °C, respectively).[3,4] In the ZrO_2–Sc_2O_3 solid solution system, an increase in the amount of scandium promotes a decrease in the phase transition temperature.[4] Thus, the replacement of Zr^{4+} by a larger Sc^{3+} cation creates oxygen vacancies and increases oxygen-ion conductivity.[5] Additional co-doping of the ZrO_2–Sc_2O_3 system with other rare earth element (REE) oxides stabilizes transport characteristics at high operating temperatures while maintaining the highly conductive cubic phase of ZrO_2.[5,6] Cubic ZrO_2 is formed by structuring solid films from nanocrystallites.[7] At the same time, the solubility range of Sc_2O_3 was expanded from 11 to 17.5 mol% in ZrO_2.[8]

Recently, pure and doped ZrO_2 have been widely considered in heterogeneous catalysis for oxidation of organic hydrocarbons using solar energy or UV radiation.[9–11] By promoting oxygen adsorption and electron absorption on the surface of an oxide material, REEs and scandium, which create additional electronic levels in the middle of the forbidden zone, improve the energy systems of photochemical water conversion in hydrogen technology and increase photodegradation activity in removing organic pollutants from water and air.[9,12]

Practically significant properties of such materials (specific surface area, degree of defectivity, porosity, size, morphology, and internal architecture of aggregates) are determined by the way of their synthesis.[13–15] At the same time, nanostructures in which the introduction of REEs additionally prevents the growth of crystallites often are more photoactive.[11] Moreover, it is necessary to know effective dopant levels and synthesis temperatures to control phase transformations.

The synthesis of oxides using individual complex compounds with an easily degradable organic ligand as precursors makes it possible to obtain complex oxides in a nanodispersed state with controlled particle morphology.[15,16]

The aim of this work was to prepare $Zr_{1-x}Sc_xO_{2-\delta}$ ($0 < x \leqslant 0.1$) solid solutions with enhanced photoactivity. A mixed $Zr_{1-x}Sc_xO(HCOO)_2{\cdot}2H_2O$ formate used as a precursor was synthesized under solvothermal conditions at 60 °C according to the hypothetical reaction

$$Zr_{1-x}Sc_x(NO_3)_4{\cdot}2H_2O + 3HCOOH \rightarrow Zr_{1-x}Sc_xO(HCOO)_2{\cdot}2H_2O + 4NO_2 + CO_2 + 3H_2O. \quad (1)$$

$Zr_{1-x}Sc_x(NO_3)_4{\cdot}2H_2O$ was obtained by interaction of concentrated HNO_3 with stoichiometric mixtures of $Zr(OH)_2CO_3{\cdot}5H_2O$ and Sc_2O_3. According to XRPD, IR, and SEM data,† the mixed formate $Zr_{1-x}Sc_xO(HCOO)_2{\cdot}2H_2O$ was a phase of variable composition, which crystallized as lamellar white crystals with average sizes of 200 × 500 nm [Figure 1(*a*)]. Typical diffraction spectra showed that as-prepared $Zr_{1-x}Sc_xO(HCOO)_2{\cdot}2H_2O$ crystallized in rhombic syngony (space group *Cmcm*) [Figure 1(*b*), curve *1*], similar to that

† X–ray powder diffraction (XRD–7000 diffractometer, Shimadzu, Japan) using CuKα radiation in the 2θ range from 5° to 80° with a step of 0.03° was employed. The morphological peculiarities were examined by scanning electron microscopy (SEM) on a Tescan Vega Compact microscope with an EDS X-max Oxford Instruments. Differential scanning calorimetry (DSC) and thermogravimetric analysis (TG) were performed on a Setsys Evolution thermoanalyser (Setaram, France) in air at a temperature change rate of 10 K min^{-1} in the temperature range 20–1000 °C; the reference standard was aluminum oxide. IR spectra were recorded on a Nicolet 6700 Thermo Scientific spectrometer at 400–4000 cm^{-1}. The photocatalytic activity of the products was evaluated by oxidation of benzene-1,4-diol under UV irradiation. The solutions were irradiated in quartz cuvettes using a BUV-15 lamp (λ_{max} = 253 nm). The concentration of hydroquinone was monitored by a voltammetric method using a PU-1 polarography.[14]

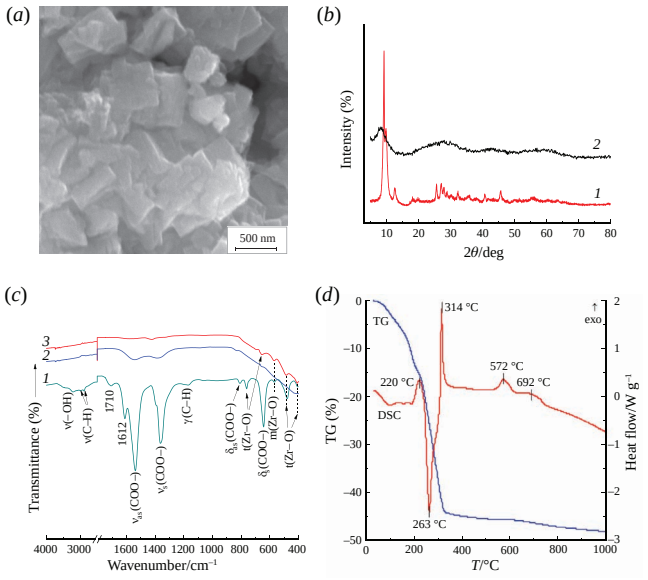

Figure 1 (*a*) SEM image of $Zr_{1-x}Sc_xO(HCOO)_2{\cdot}2H_2O$ formate at $x = 0.05$; (*b*) XRD patterns of (*1*) the initial formate and (*2*) the product of its reprecipitation; (*c*) IR spectra of (*1*) the initial formate and its thermolysis products at (*2*) 500 and (*3*) 700 °C; (*d*) heating TG and DSC curves for the formate $Zr_{0.95}Sc_{0.05}O(HCOO)_{2-\delta}{\cdot}2H_2O$.

described previously.[17] The formate obtained was soluble in water with the formation of a real solution. After re-precipitation by evaporation of water, an X-ray amorphous transparent film was formed due to the polymerization of formate without reverse crystallization [Figure 1(*b*), curve *2*]. According to published data,[12–14] carboxylate-substituted $Zr_6O_4(OH)_4(OOCR)_{12}$ clusters belong to the group of metal oxo clusters with high symmetry containing bridging and chelate carboxylate ligands. The vibrational spectra of $Zr_{1-x}Sc_xO(HCOO)_2{\cdot}2H_2O$ [Figure 1(*c*)] confirmed the presence of short-term Zr–O bonds and COO^- and CH^- groups in the $HCOO^-$ anion. In a range of 3200–3500 cm^{-1}, a broad and very weak band corresponded to stretching vibrations and a band at 1612 cm^{-1} was due to bending vibrations of O–H bonds of water. Two types of formate groups were identified in the test sample: a band at 898 cm^{-1} was related to δ(C–H), while bands at 1351 and 1708 cm^{-1} referred to $\nu_{as}(COO^-)$ and ν(C=O) within the weakly bound formate ion. The remaining bands were assigned to formate groups coordinated by the Zr(Sc) atom. The stretching vibrations of C–H bonds were very weak in the region of 2800–2950 cm^{-1}. An intense narrow band at 1540 cm^{-1} was responsible for the asymmetric stretching vibrations of C–O bonds in the COO^- group. The band at 1350 cm^{-1} with a shoulder at 1400 cm^{-1} corresponded to the symmetrical stretching vibrations of C–O bonds in the COO^- group. A very weak absorption band at 1080 cm^{-1} was associated with out-of-plane bending vibrations of C–H bonds. The absorption bands at 820 and 640 cm^{-1} corresponded to δ(COO^-). The band at 760 cm^{-1} can be attributed to δ(COO^-) in the weakly bound formate ion and to vibrations of Zr–O bonds, as well as the bands at 560 and 480 cm^{-1}. The above IR spectra of the thermolysis products of $Zr_{1-x}Sc_xO(HCOO)_2{\cdot}2H_2O$ ($x = 0.05$) showed incomplete removal of $HCOO^-$ at 500 °C [Figure 1(*c*), curve 2].

The spectra contained a band at 480 cm^{-1} due to the tetragonally non-transformable t′′-phase (space group $P4_2/nmc$), which was characterized by the tetragonality parameter $c/a = 1$ characteristic of a cubic structure.[15,16] However, in contrast, the tetragonal t′′-phase was characterized by an insignificant displacement of oxygen ions. According to TG analysis data, the decomposition of $Zr_{1-x}Sc_xO(HCOO)_{2-\delta}{\cdot}2H_2O$ proceeded sequentially in two main steps [Figure 1(d)]. The gradual removal of crystallization water at 220–350 °C with the simultaneous decomposition of $HCOO^-$ groups was manifested by an endothermic effect that results in an intense exothermic effect of oxidation to CO_2 at 314 °C. The total weight loss of this process was 45.2 wt%. The decomposition was completed at 750–800 °C by the formation of $Zr_{1-x}Sc_xO_{2-\delta}$. The weight loss in a temperature range of 600–800 °C was 2.6 wt%. At this temperature, the final removal of carbonate groups was accompanied by two exothermic effects in the DSC curve. The weight loss of complete thermal decomposition of $Zr_{1-x}Sc_xO(HCOO)_2{\cdot}2H_2O$ to form $Zr_{1-x}Sc_xO_2$ was 47.7 wt% (theoretical loss is 48 wt%). Therefore, the thermolysis of $Zr_{1-x}Sc_xO(HCOO)_2{\cdot}2H_2O$ can be represented as the sequence

$$Zr_{1-x}Sc_xO(HCOO)_2{\cdot}2H_2O \xrightarrow{250–350\ ^\circ C} Zr_{1-x}Sc_xO(HCOO)_2 \longrightarrow Zr_{1-x}Sc_xO(CO_2)_2 \xrightarrow{600–800\ ^\circ C} Zr_{1-x}Sc_xO_2. \quad (2)$$

X-ray diffraction of the thermolysis products of $Zr_{1-x}Sc_xO(HCOO)_2{\cdot}2H_2O$ in air at 700 °C showed that $Zr_{1-x}Sc_xO_2$ was formed in two main modifications: monoclinic (m, space group $P2_1/c$) and tetragonal (t, space group $P4_2/nmc$) [Figure 2(*a*)]. Scandium doping promoted an almost linear increase in the amount of tetragonal phase up to 56% at $x = 0.1$, while undoped ZrO_2 crystallized by 90% in the monoclinic syngony (Figure S1, see Online Supplementary Materials). As the scandium content of the m-phase increased, the unit cell parameter a_m increased linearly from 5.157 to 5.163 Å, while the parameters b_m and V_m decreased and the parameter c_m remained constant (Figure S2) due to the incorporation of scandium into the m-ZrO_2 structure. For t-ZrO_2, the parameter a_t slightly increased from 3.601 to 3.605 Å (Figure S3). Note that the tetragonal and monoclinic phases can be represented as the derivatives of a cubic fluorite-type phase ($Fm\bar{3}m$) with the cell parameter $a = 5.09–5.26$ Å. This structure is a superposition of two cubic sublattices formed by zirconium cations and oxygen anions.[20,21]

The morphology of the thermolysis products retained the original precursor type [Figure 2(*b*)]. The SEM image of $Zr_{0.95}Sc_{0.05}O_{2-\delta}$ shows that the thermolysis product contained almost spherical agglomerates of lamellar crystals about 120 × 350 nm in size, prone to cross-joining. The introduction of scandium had no effect on the morphology and size of both the initial crystallites and their agglomerates. The average size of $Zr_{0.95}Sc_{0.05}O_{2-\delta}$ crystallites in the smaller direction was 107 nm, and the size of agglomerates reached 1108 nm (Figure S4

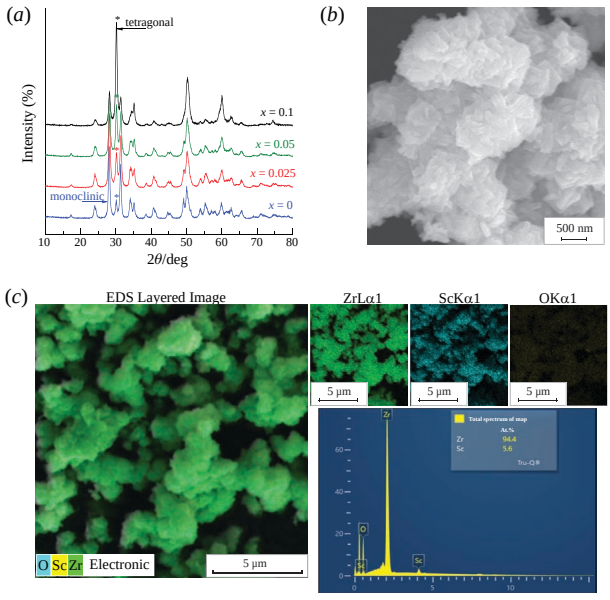

Figure 2 (*a*) Diffractograms of $Zr_{1-x}Sc_xO_{2-\delta}$ at $0 < x \leqslant 0.1$; (*b*) SEM image and (*c*) EDS data analysis of $Zr_{1-x}Sc_xO_{2-\delta}$ at $x = 0.05$.

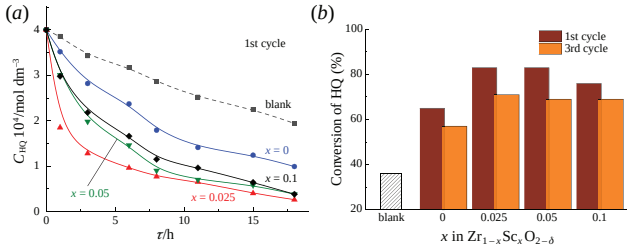

Figure 3 Photooxidation of HQ under UV stimulation in the presence of $Zr_{1-x}Sc_xO_{2-\delta}$: (*a*) kinetic curves of the first cycle; (*b*) degree of HQ conversion in the first and third cycles for 10 h.

and S5). According to EDS results, the elemental composition of the sample corresponded to the formula $Zr_{0.95}Sc_{0.05}O_{2-\delta}$ [Figure 2(*c*)]. The mapping method showed a uniform distribution of elements (Zr, Sc, and O) over the SEM image area.

The photocatalytic properties of $Zr_{1-x}Sc_xO_{2-\delta}$ ($0 < x \leqslant 0.1$) solid solutions were studied in the oxidation reaction of benzene-1,4-diol [hydroquinone (HQ)] in aqueous solutions under stimulation with light at the wavelength λ_{max} = 253 nm (UV range). The concentration of hydroquinone was monitored by voltammetry. Under these conditions, the solid solutions exhibited appreciable photocatalytic activity depending on the Sc concentration [Figure 3(*a*)]. The stability of the catalyst performance was evaluated in three consecutive oxidation cycles. An increase in the concentration of scandium in the ZrO_2 matrix slightly reduced the photocatalytic properties, especially in the third cycle of photooxidation [Figure 3(*b*)]. The best properties in the first cycle, exceeding by a factor of 2 the performance of a commercial Degussa P25 catalyst,[22] were shown by the $Zr_{0.975}Sc_{0.025}O_{2-\delta}$ solid solution (Table 1). Increasing the amount of a tetragonal ZrO_2 phase had a negative effect, as noted by Teeparthi *et al.*[10]

The use of $Zr_{1-x}Sc_xO_{2-\delta}$ ($0 < x \leqslant 0.1$) solid solutions obtained by low-temperature thermolysis of $Zr_{1-x}Sc_xO(HCOO)_{2-\delta}\cdot 2H_2O$ formates in UV-stimulated oxidative catalysis led to a significant reduction in the oxidation of benzene derivatives, especially noticeable in cycle 1 (Table 1).

Thus, the use of the formate $Zr_{1-x}Sc_xO(HCOO)_2\cdot 2H_2O$ as a precursor in low-temperature thermolysis yielded $Zr_{1-x}Sc_xO_{2-\delta}$ ($0 < x \leqslant 0.1$) in two allotropic modifications. Scandium favored the formation of a tetragonal phase, the closest to cubic phase. Undoped ZrO_2 oxide crystallized at 700 °C mainly in a monoclinic syngony, which differed from the tetragonal one by a shear deformation of the entire unit cell. The formation of more disordered m-phase ZrO_2 during the pseudomorphic thermal conversion of $Zr_{1-x}Sc_xO(HCOO)_2\cdot 2H_2O$ implied the presence of a significant number of intrinsic structural defects. At heterovalent substitution, scandium as an effective acceptor impurity in the zirconium oxide structure stimulated an increase in the photoactivity of ZrO_2.

Table 1 Reaction rate constants (k_s) and half-reaction times ($\tau^{1/2}$)[a] of HQ oxidation by $Zr_{1-x}Sc_xO_{2-\delta}$ samples.

Catalyst	Cycle	$k_s \times 10^5/s^{-1}$	$\tau^{1/2}/h^{1/2}$
Without catalyst	1	1.34 ± 0.12	16.2
Degussa	1	4.37 ± 0.65	4.9
x = 0	1	2.69 ± 0.51	7.2
	2	2.02 ± 0.49	9.5
	3	3.10 ± 1.35	6.2
x = 0.025	1	8.04 ± 0.82	2.4
	2	4.82 ± 0.75	4.0
	3	4.43 ± 1.30	4.3
x = 0.05	1	5.12 ± 1.22	3.8
	2	5.36 ± 1.28	3.6
	3	3.16 ± 1.51	6.1
x = 0.1	1	4.69 ± 1.38	4.1
	2	5.47 ± 1.38	3.5
	3	4.85 ± 1.26	3.8

[a] k_s and $\tau^{1/2}$ were calculated from the equation $k_s\,\tau = -\ln(C_\tau/C_0)$, where C_0 and C_τ are the initial concentrations after dark adsorption and residual HQ concentrations at a certain irradiation time, respectively.

The work was supported by the Russian Science Foundation, grant no. 24-29-20278, https://rscf.ru/en/project/24-29-20278/.

Online Supplementary Materials

Supplementary data associated with this article can be found in the online version at doi: 10.1016/j.mencom.2024.09.005.

References

1 D. Udomsilp, C. Lenser, O. Guillon and N. H. Menzler, *Energy Technol.*, 2021, **9**, 2001062.
2 A. A. Chernyshev, D. N. Lytkina, A. S. Buiakov, S. N. Kulkov and I. A. Kurzina, *Mendeleev Commun.*, 2021, **31**, 881.
3 M. Mosavari, A. Khajehhaghverdi and R. M. Aghdam, *Inorg. Chem. Commun.*, 2023, **157**, 111293.
4 H. Fujimori, M. Yashima, M. Kakihana and M. Yoshimura, *J. Am. Ceram. Soc.*, 1998, **81**, 2885.
5 J. W. Fergus, *J. Power Sources*, 2006, **162**, 30.
6 A. O. Zhigachev, V. V. Rodaev, D. V. Zhigacheva, N. V. Lyskov and M. A. Shchukina, *Ceram. Int.*, 2021, **47**, 32490.
7 Y. Guan, J. Zhou, H. Zhong, W. Wang, Z. Zhang and F. Luo, *J. Adv. Ceram.*, 2023, **12**, 822.
8 V. Danchuk, M. Shatalov, M. Zinigrad, A. Kossenko, T. Brider, L. Le, D. Johnson, Y. M. Strzhemechny and A. Musin, *Nanomaterials*, 2024, **14**, 708.
9 E. Gaggero, P. Calza, E. Cerrato and M. C. Paganini, *Catalysts*, 2021, **11**, 1520.
10 S. R. Teeparthi, E. W. Awin and R. Kumar, *Sci. Rep.*, 2018, **8**, 5541.
11 S. Kumar and A. K. Ojha, *J. Alloys Compd.*, 2015, **644**, 654.
12 A. Ahmad, J. A. Shah, S. Buzby and S. I. Shah, *Eur. J. Inorg. Chem.*, 2008, **6**, 948.
13 I. A. Kovalev, A. A. Petrov, O. A. Ibragimova, A. V. Shokod'ko, A. S. Chernyavskii, E. A. Goodilin, K. A. Solntsev and A. B. Tarasov, *Mendeleev Commun.*, 2018, **28**, 541.
14 A. N. Bugrov and O. V. Almjasheva, *Nanosyst.: Phys. Chem. Math.*, 2013, **4**, 810.
15 O. I. Gyrdasova, E. V. Vladimirova, L. Yu. Buldakova, M. Yu. Yanchenko and A. V. Dmitriev, *Mendeleev Commun.*, 2023, **33**, 368.
16 O. I. Gyrdasova, L. A. Pasechnik, V. N. Krasil'nikov, T. P. Gavrilova, I. V. Yatsyk, Y. V. Kuznetsova, M. O. Kalinkin and M. V. Kuznetsov, *Water Environ. Res.*, 2023, **95**, e10956.
17 W. Liang, R. Babarao, M. J. Murphy and D. M D'Alessandro, *Dalton Trans.*, 2014, **44**, 1516.
18 U. Schubert, *Coord. Chem. Rev.*, 2022, **469**, 214686.
19 Y. Bai, Y. Dou, L.-H. Xie, W. Rutledge, J.-R. Li and H.-C. Zhou, *Chem. Soc. Rev.*, 2016, **45**, 2327.
20 I. O. Fábregas, M. Reinoso, E. Otal and M. Kim, *J. Eur. Ceram. Soc.*, 2016, **36**, 2043.
21 M. Yashima, K. Ohtake, H. Arashi, M. Kakihana and M. Yoshimura, *J. Appl. Phys.*, 1993, **74**, 7603.
22 T. I. Chupakhina, R. M. Eremina, O. I. Gyrdasova, M. Yu. Yanchenko, L. Yu. Buldakova, I. V. Yatsyk, T. P. Gavrilova, Yu. A. Deeva, A. A. Sukhanov, I. V. Baklanova and A. M. Uporova, *J. Korean Ceram. Soc.*, 2024, **61**, 623.

Received: 23rd April 2024; Com. 24/7475